Molecular hydrogen formation on interstellar PAHs through Eley-Rideal abstraction reactions

Nolan Foley[1], S. Cazaux[2,3], D. Egorov[1], L.M.P.V. Boschman[1,4], R. Hoekstra[1] and T. Schlathölter[1] [*]

[1] *Zernike Institute for Advanced Materials, University of Groningen, Nijenborgh 4, 9747 AG Groningen, The Netherlands*
[2] *Faculty of Aerospace Engineering, Delft University of Technology, Kluyverweg 1, 2629 HS, Delft, The Netherlands*
[3] *University of Leiden, P.O. Box 9513, NL, 2300 RA, Leiden, The Netherlands.*
[4] *Kapteyn Astronomical Institute, University of Groningen, Landleven 12, 9747 AD, Groningen, The Netherlands*

ABSTRACT

We present experimental data on H_2 formation processes on gas-phase polycyclic aromatic hydrocarbon (PAH) cations. This process was studied by exposing coronene radical cations, confined in a radio-frequency ion trap, to gas phase H atoms. Sequential attachment of up to 23 hydrogen atoms has been observed. Exposure to atomic D instead of H allows one to distinguish attachment from competing abstraction reactions, as the latter now leave a unique fingerprint in the measured mass spectra. Modeling of the experimental results using realistic cross sections and barriers for attachment and abstraction yield a 1:2 ratio of abstraction to attachment cross sections. The strong contribution of abstraction indicates that H_2 formation on interstellar PAH cations is an order of magnitude more relevant than previously thought.

Key words: astrochemistry – molecular processes – methods: laboratory: molecular – ISM: molecules

1 INTRODUCTION

The formation of molecular hydrogen in the interstellar medium (ISM) is a topic of ongoing debate (see recent review Wakelam et al. (2017)). As molecular hydrogen is the most abundant molecule in the universe and plays a key role in many astrophysical processes, a proper understanding of the processes that lead to its formation is of great interest. A number of potential formation processes have already been explored. While gas phase routes to H_2 formation have been found to be inefficient, formation on interstellar dust grains has been identified as one possible mechanism (Oort & van de Hulst 1946; Gould & Salpeter 1963). Another possible route to molecular hydrogen formation is on interstellar polycyclic aromatic hydrocarbons (PAHs) (Bauschlicher 1998; Hirama et al. 2004; LePage et al. 2009; Mennella et al. 2012; Boschman et al. 2012; Thrower et al. 2012). A variety of objects inside and outside our galaxy exhibit spectra crowded with unidentified lines. These lines can be seen in absorption in the optical (diffuse interstellar bands: DIBS) and in emission in the infrared (aromatic infrared bands: AIB). Ubiquitous interstellar AIB are now commonly considered to be carried by PAHs. These PAHs are typically at least partially hydrogenated (Schutte et al. 1993; Bernstein

et al. 1996). Assuming DIBS to be due to PAH-based species as well, it is most likely that part are present in protonated form or as superhydrogenated cations, which feature the observed transitions in the visible (LePage et al. 1997; Snow et al. 1998; Hammonds et al. 2009).

Atomic hydrogen impacting on PAH may undergo an attachment reaction and become attached to the molecule. Sequences of these addition reactions, with s additional H atoms, are of the type

$$[PAH + sH] + H \rightarrow [PAH + (s + 1)H], \quad \Delta M = +1 \quad (1)$$
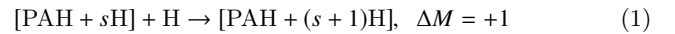
are referred to as hydrogenation sequences, and leave the PAH in a state of superhydrogenation and increase its mass M by 1. Recent experimental and theoretical research on trapped coronene radical cations $C_{24}H_{12}^+$ revealed that in the gas-phase and at $T = 300$ K, hydrogenation proceeds through a specific sequence of well-defined atomic sites. Reaction barriers and binding energies lead to odd - even oscillations in the observed superhydrogenation states, and magic numbers of particularly high intensity for the attachment of $n = 5$, 11, and 17 extra H atoms (Boschman et al. 2012; Cazaux et al. 2016).

Superhydrogenation dramatically alters the response of neutral and ionic gas-phase PAHs in various astrochemically relevant interaction processes. Attachment of small numbers of H atoms to coronene cations can for instance

[*] Contact e-mail: t.a.schlatholter@rug.nl

arXiv:1808.09192v1 [astro-ph.GA] 28 Aug 2018

quench photoionization-induced H loss from a $C_{24}H_{12}^+$ precursor cation (Reitsma et al. 2014, 2015). For superhydrogenation of neutral pyrene molecules, an opposite effect was observed. The C-backbone is weakened and fragmentation upon ion collisions or photoionization is increased (Wolf et al. 2016; Gatchell et al. 2015). Attachment of a single H atom to a PAH radical cations has a dramatic influence on its IR spectrum (Knorke et al. 2009) and substantially decreases the HOMO-LUMO gap (Pathak & Sarre 2008).

In 1998 a second type of H reaction with PAH molecules was proposed (Bauschlicher 1998), which was experimentally confirmed in 2012 through hydrogenation experiments on supported PAH thin films by Mennella et al. (Mennella et al. 2012). In these so-called direct abstraction reactions of the Eley-Rideal type

$$[PAH + sH] + H \rightarrow [PAH + (s-1)H] + H_2, \quad \Delta M = -1 \qquad (2)$$
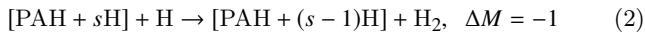
the incoming H atom does not get bound to the PAH molecule, but rather reacts with an H atom already present in the hydrogenated PAH, to directly desorb as an H_2 molecule. In these experiments on solid PAH films the abstraction channel is determined to be more than an order of magnitude weaker than H attachment, with the reaction cross sections for abstraction and attachment being respectively 0.06 Å^2 and 1.1 Å^2 corresponding to a ratio between abstraction and attachment of $\approx 1 : 20$ (Mennella et al. 2012).

In the following, we study H abstraction reactions on gas phase coronene cations, $C_{24}H_{12}^+$. It should be noted that coronene is not a major species in the interstellar medium (Hirama et al. 2004), but it is used as one of the prototypical PAHs in related astrolaboratory research (Boschman et al. 2012; Cazaux et al. 2016; Rauls & Hornekaer 2008; Boschman et al. 2015; Jochims et al. 1994; Ling & Lifshitz 1998) because it is fairly large and has a compact shape, making it relatively easy to work with, and it is commercially available in large quantities. By comparing the mass spectra obtained from $C_{24}H_{12}^+$ exposure to $T = 300$ K H and D beams, respectively, direct evidence for the occurrence of abstraction reactions is observed. The modeling of the measured mass spectra with a time-dependent rate equation model indicates a relative cross section for abstraction that is about an order of magnitude larger than previously thought.

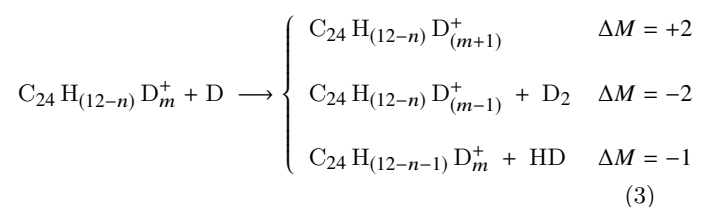## 2 EXPERIMENT

2.1 Concept of the experiment

The hydrogenation of coronene cations is predominantly determined by the alternating heights of the energy barriers for hydrogen addition. Even numbered superhydrogenation states can be subject to barrierless hydrogenation, whereas hydrogen attachment to odd-numbered superhydrogenation states involves a reaction barrier. As a result, all (closed shell) odd-numbered superhydrogenation states are more stable than the (radical) even-numbered states and occur significantly more often. A typical mass spectrum consists of dominating peaks at $M = 301, 303, 305$ etc. On top of that, "magic" stages of superhydrogenation are observed for the attachment of 5, 11, and 17 H atoms, corresponding to
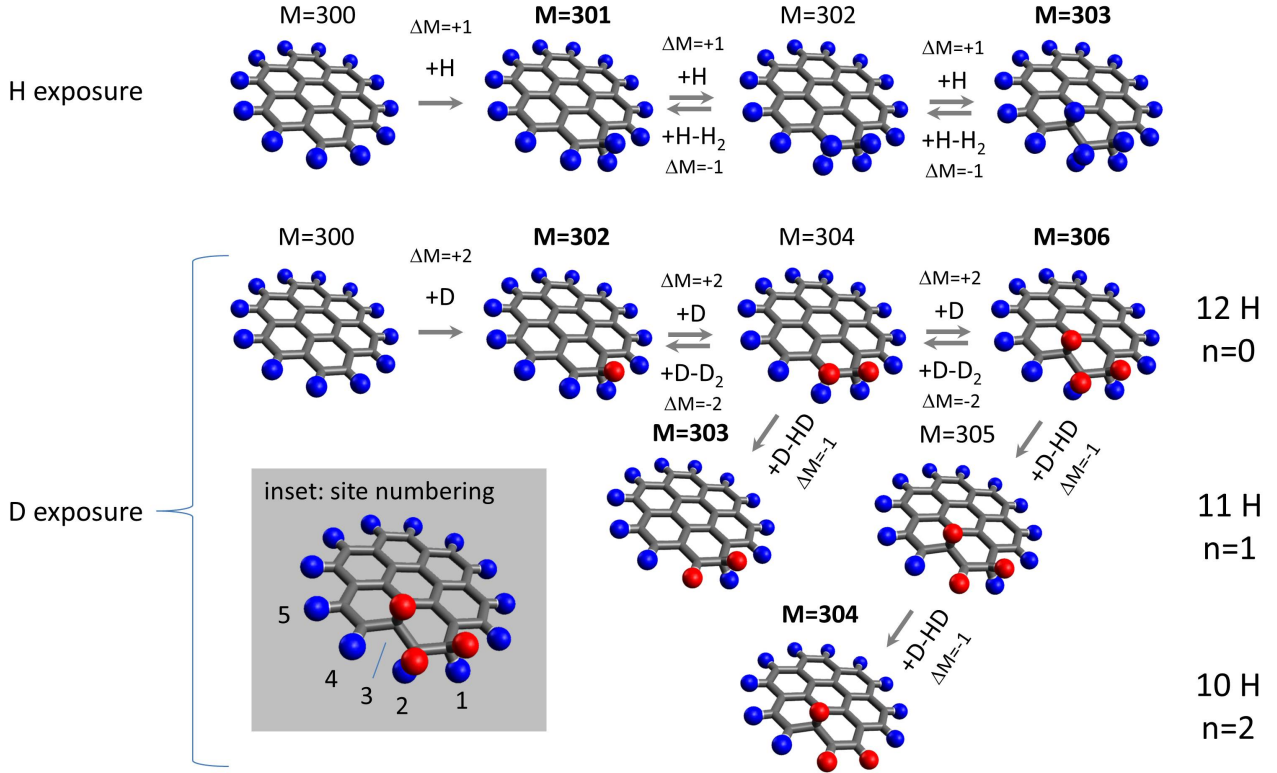
hydrogenation stages which have particularly high binding energies (Cazaux et al. 2016).

In principle, an incoming H atom can interact with every C site in a coronene cation. As a first step, the attachment on one of the outer edge positions is energetically most favorable and thus most likely (Mennella et al. 2012; Cazaux et al. 2016). As a result, two H atoms are attached to a single carbon atom, which we shall refer to as the position being doubly occupied. Figure 1 illustrates the initial hydrogenation and abstraction steps for a coronene cation. In the top row, the case of H exposure is sketched. The first H attachment leads to a doubly occupied outer edge site and results in a mass increase by one unit into $M = 301$. Previous experimental studies have shown that this process quickly transfers the entire $C_{24}H_{12}^+$ population into $C_{24}H_{13}^+$ (Boschman et al. 2012). This implies that the probability of abstraction from $C_{24}H_{13}^+$ is negligibly small. Attachment of a second H atom leads to double occupation of the adjacent outer edge site and a molecular mass of $M = 302$. From here on further hydrogenation competes with abstraction, if an impinging H atom impacts on a previously created doubly occupied site and undergoes an Eley-Rideal reaction (Mennella et al. 2012) with one of the H atoms attached to the site. This leads to the release of a neutral H_2 molecule which corresponds to the net loss of an H atom by the molecule (see eq. 2).

From a mass spectrometric perspective, it is important to realize that since hydrogenation and abstraction shift the mass of a superhydrogenated coronene cation by +1 and -1, respectively, it is not possible to establish whether a $C_{24}H_{12+n}^+$ originates from $C_{24}H_{12+(n-1)}^+$ via H attachment or from $C_{24}H_{12+(n+1)}^+$ via H abstraction. This explains why abstraction reactions remained obscured thus far in gas phase hydrogenation experiments. Furthermore, as abstraction counteracts the mass shift towards higher masses driven by hydrogenation, the rates for H addition might well be underestimated.

In order to overcome this problem and quantify the relative contribution of abstraction reactions on gas-phase coronene cations, the cations can be exposed to atomic D (^{2}H) rather than H (^{1}H). Addition and abstraction of atomic D then change the mass of the molecular precursor by +2 and -2, respectively. Except for the twice as large step size in mass, this yields a similar spectrum as for hydrogen. The doubly occupied sites, however, are initially occupied by an H and a D atom, i.e. the abstraction reaction can also involve an H atom, leading to a mass change of only -1. For our prototypical system, coronene with an initial mass of 300, the appearance of molecular ions with odd mass numbers is a direct signature of such an abstraction. More specific for a coronene cation $C_{24}H_{(12-n)}D_m^+$ that has lost n of its initial H atoms by HD abstraction and contains m additional D atoms the following generic reactions need to be considered:

$$C_{24}H_{(12-n)}D_m^+ + D \longrightarrow \begin{cases} C_{24}H_{(12-n)}D_{(m+1)}^+ & \Delta M = +2 \\ C_{24}H_{(12-n)}D_{(m-1)}^+ + D_2 & \Delta M = -2 \\ C_{24}H_{(12-n-1)}D_m^+ + HD & \Delta M = -1 \end{cases}$$

$$(3)$$

Figure 1. Schematic representation of the reaction sequences for subsequent H (top row) or D (bottom row network) interactions with a coronene cation. H atoms are marked in blue and D atoms in red. Only a selection of possible attachment (+H, +D) and abstraction (+H-H$_2$, +D-D$_2$, +D-HD) processes are indicated. The third atom is attached to an inner edge site, as indicated by recent IR spectroscopy data (Schlathölter et al. 2018) and not an outer edge site as previously predicted (Cazaux et al. 2016). The masses of systems that possess an odd total number of H+D atoms are given in bold letters.

The reaction network driven by thermal D exposure described by eq.3 is schematically illustrated in the bottom part of Figure 1. As for H, it is assumed that the singly hydrogenated cation is not undergoing significant abstraction reactions. In the figure H atoms are marked in blue and D atoms in red. From the figure and eq. 3 it is clear that for attachment and abstraction of a D atom the systems changes mass in steps of ±2 and stays in the same row. Loss of an H atom (HD abstraction) moves the molecular system one row down. The rows are characterized by the number of H atoms removed from the precursor coronene cation. The rows with odd numbers of H atoms abstracted correspond to odd-mass cations and are a direct signature of abstraction which allow us to determine both attachment and abstraction cross sections and barriers.

2.2 Experimental implementation

The coronene radical cations were produced by means of electrospray ionization (ESI) from a coronene solution in methanol. Admixture of AgNO$_3$ to the solution facilitates charge transfer from C$_{24}$H$_{12}$ to Ag$^+$. The C$_{24}$H$_{12}^+$ beam generated by the ESI source was then phase space compressed in a RF ion funnel and mass selected in a RF quadrupole mass filter. The ions were then trapped in a 3D RF ion trap at ambient temperature (Bari et al. 2011; Egorov et al. 2016). Note, that the substantial binding energy of atomic hydro-

gen on coronene cations (2 - 3.5 eV (Cazaux et al. 2016)) is deposited into the molecular system with every attachment event. At the same time, the system is subject to cooling by photon emission and fragmentation processes. The resulting internal excitation depends on the experimental conditions but only marginally on the initial temperature, as discussed elsewhere (Rapacioli et al. 2018).

Molecular hydrogen or deuterium gas was dissociated in a Slevin-type discharge source operated at an RF frequency of 27 MHz (Hoekstra et al. 1991; Boschman et al. 2012; Reitsma et al. 2014). The gas was cooled through collisions with a water-cooled sleeve and guided through Teflon tubes into the RF trap holding the C$_{24}$H$_{12}^+$ target. For both hydrogen and deuterium exposures, exposure times were set to 0.15, 0.5, 1, 3, 6, 9, 12, 15, and 40 s in order to get broad view of the resulting superhydrogenation states. All hydrogenation and deuteration measurements were performed under otherwise identical experimental conditions.

Before the hydrogenation experiments, a reference measurement was made of the pristine coronene cation sample. The resulting mass spectrum can be found in the top panel of Figure 2. The main feature of the mass spectrum is the C$_{24}$H$_{12}^+$ precursor ion with M = 300 amu. A weak peak at M = 301 is due to ^{12}C$_{23}^{13}$C H$_{12}^+$. This peak is due to the naturally occurring ^{13}C isotope. In order to correct for this peak in the analysis of subsequent measurements, the ratio between the main coronene mass peak and this isotope

peak was calculated. This ratio was used during calculations on all mass peaks in the subsequent measurements to correct for the presence of this isotope peak. It is of note that the isotopic contribution is much less than its natural fraction of almost 25%, due to the mass filtering by the RF quadrupole. Tighter filtering starts to reduce the number of $C_{24}H_{12}^+$ cations of $M = 300$ as well, thereby hampering performing experiments with sufficient statistics.

2.3 Results

The left panel in fig. 2 shows the evolution of the mass spectrum with increasing H exposure time. The pressure in the RF-trap chamber was at $p = 1.5 \times 10^{-6}$ mbar. Already after an H exposure time $t_{exp} = 0.15$ s, more than half of the trapped ions are in the singly superhydrogenated state ($M = 301$, +H). For $t_{exp} = 1$ s, almost the entire trap content is singly superhydrogenated and a small feature due to triple superhydrogenation emerges ($M = 303$, +3H). With increasing t_{exp}, the ratio between +H and +3H shifts towards the latter one and at $t_{exp} = 6$ s, the next odd superhydrogenation appears ($M = 305$, +5H). At an exposure time of $t_{exp} = 9$ s, first traces of 7-fold superhydrogenation show up ($M = 307$, +7H). In between the odd-mass peaks, the weak intensity at even mass numbers is mostly due to the presence of ^{13}C in the precursor ion. The evolution towards the expected superhydrogenation pattern with its pronounced odd-even oscillation is evident. As discussed in the introduction, for atomic H exposure H abstraction remains hidden in the mass spectra as it leads to formation of molecular cations of identical masses.

The right panel of fig. 2 shows the corresponding results for D exposure at otherwise identical conditions. For the shortest exposure time of 0.15 s, results for H and D exposure only differ in mass shift. In both cases, more than half of the $C_{24}H_{12}^+$ population has been transferred to the singly superhydrogenated or superdeuterated state. As discussed in the introduction, abstraction does not play a role in this step. For longer exposure times the deuteration spectra are much more complex than the hydrogenation ones. The generic trends, and especially the additional information contained in the more complex deuterium spectra, will be illustrated for the cases of 1 and 3 s exposure.

For exposures times longer than 1 s, HD abstraction occurs, resulting in the appearance of peaks in between the ones corresponding to the attachment of 1 and 3 D atoms at $M = 302$ and $M = 306$, respectively. For 1 s exposure, peaks at $M = 303$ and $M = 304$ are clearly visible. As illustrated in figure 1, the production of $M = 303$ requires the subsequent attachment of 2 D atoms followed by a HD abstraction event. The peak at $M = 304$ requires the attachment of 3 D atoms and 2 HD abstraction events.

For $t_{exp} = 3$ s, hydrogenation of the coronene cations show singly hydrogenated species at $M = 301$, as well as triply hydrogenated species at $M = 303$. Deuteration of coronene cations, on the other hand, leads to the presence of singly and triply deuterated species at $M = 302$ and $M = 306$ respectively. However, many intermediate masses can be observed, which are resulting from abstraction reactions such as the masses $M = 303, 304,$ and 305 (+2D-H, +3D-2H, and +4D-3H, respectively). With further increase of t_{exp}, the hydrogenation pattern continues to evolve according to

the same principle: new odd superdeuteration states appear (masses $M = 310$, +5D) and subsequently become accompanied by higher mass species with higher D content and lower H content. Note that the labeling in the right panel of fig.2 is not complete and only features the most straightforward sequences leading to odd total numbers of hydrogen and deuterium atoms involved. For longer exposure time of $t_{exp} = 6$ s and $t_{exp} = 9$ s, coronene cations with 5 and then with 7 extra deuterium atoms can be seen, as well as intermediate masses due to abstraction.

To conclude, for deuterated coronene the masses of stable superhydrogenation states follow the equation:

$$M_{\text{stable}} = 300 + 2m - n, m - n = [1, 3, 5,] \qquad (4)$$

Here m represents the number of D atoms attached to the molecule, and n represents the number of H atoms that have been abstracted from the molecule. For the next section it is important to realize that the composition of a stable superhydrogenation state defines the possible subsequent abstraction reactions. For instance, after HD abstraction from a deuterated site, a subsequent D attachment leaves the site doubly occupied with D atoms and accordingly, as a next step only D_2 abstraction is possible. In general the relative importance of D_2 abstraction will increase in the course of the attachment/abstraction sequence.

3 KINETIC MODEL

3.1 Assumptions

In order to extract quantitative information on reaction cross sections and barriers from the experimental data, attachment and abstraction sequences were described with a rate-equation model. To this end, the time-evolution of each of the D-exposure peaks in the experimental data from fig. 2 up to $M = 309$ was determined by integration of Gaussian fits as a function of t_{exp}. The data is shown in fig. 3 as solid circles for each mass. To be able to reach $M = 309$ (+4D -1H) not only by D-attachment, but also by HD/D_2-abstraction, attachment up to $M = 312$ and abstraction needed to be taken into account. The precise reaction barriers and cross sections for attachment and abstraction are very likely site-dependent and could not be precisely derived from our model as this would involve too many free parameters. We chose to follow the sequence and scenario derived by experiments and DFT calculations from (Cazaux et al. 2016). In that study, the barrier for addition of the first hydrogen had been estimated as $E_{attach}^{radical} = 10$ meV, while the second hydrogenation had a higher barrier of $E_{attach}^{closed} = 30$ meV, as it described a reaction between a closed shell cation and a radical. For the subsequent D attachment steps, we used this alternation between barriers of 10 meV and 30 meV until the 6th addition. For the 6th hydrogenation, a higher barrier of 100 meV had been determined. For abstraction processes, we used the small $E_{abstract} = 10$ meV barriers determined for such reactions on graphene (Morisset et al. 2004). Based on these assumptions, a chemical network capturing the different processes was established which is reported in the appendix.
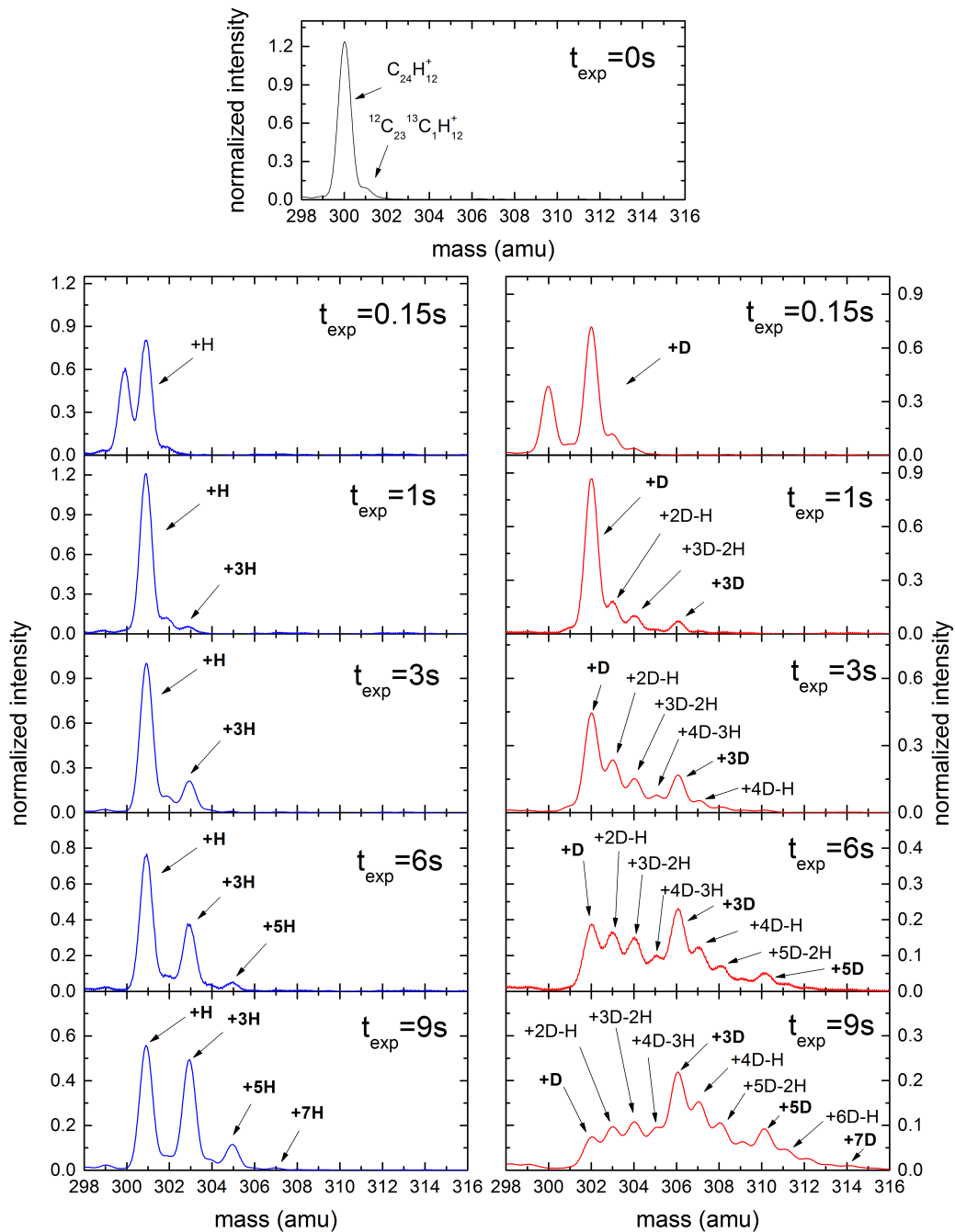
Figure 2. Top panel: Mass spectrum of the coronene radical precursor $C_{24}H_{24}^+$ featuring a small contamination of $^{12}C_{23}^{13}C_1H_{24}^+$ (see text); Left column: Evolution of the superhydrogenation pattern as a function of H exposure time t_{exp}. Right column: Evolution of the superhydrogenation pattern as a function of D exposure time t_{exp}. All distributions are normalized with respect to the total peak integral.

3.2 Results

We then compute the evolution of the yields of the different superdeuterated species using our chemical network. Our first goal is to reproduce experimental data using the values that were previously derived in other studies. First, we used cross sections for attachment (1.1 Å^2) and abstraction (0.06 Å^2) similar to the ones derived for neutral coronene

by (Mennella et al. 2012) and independent on the hydrogenation state Skov et al. (2014). In this low abstraction scenario the computations do not reproduce the even mass-numbered superdeuterated states reported in fig. 3, which imply the abstraction of a H atom by a D to form HD. In order to reproduce the experimentally observed yields of all species whose formation involved abstraction processes, the
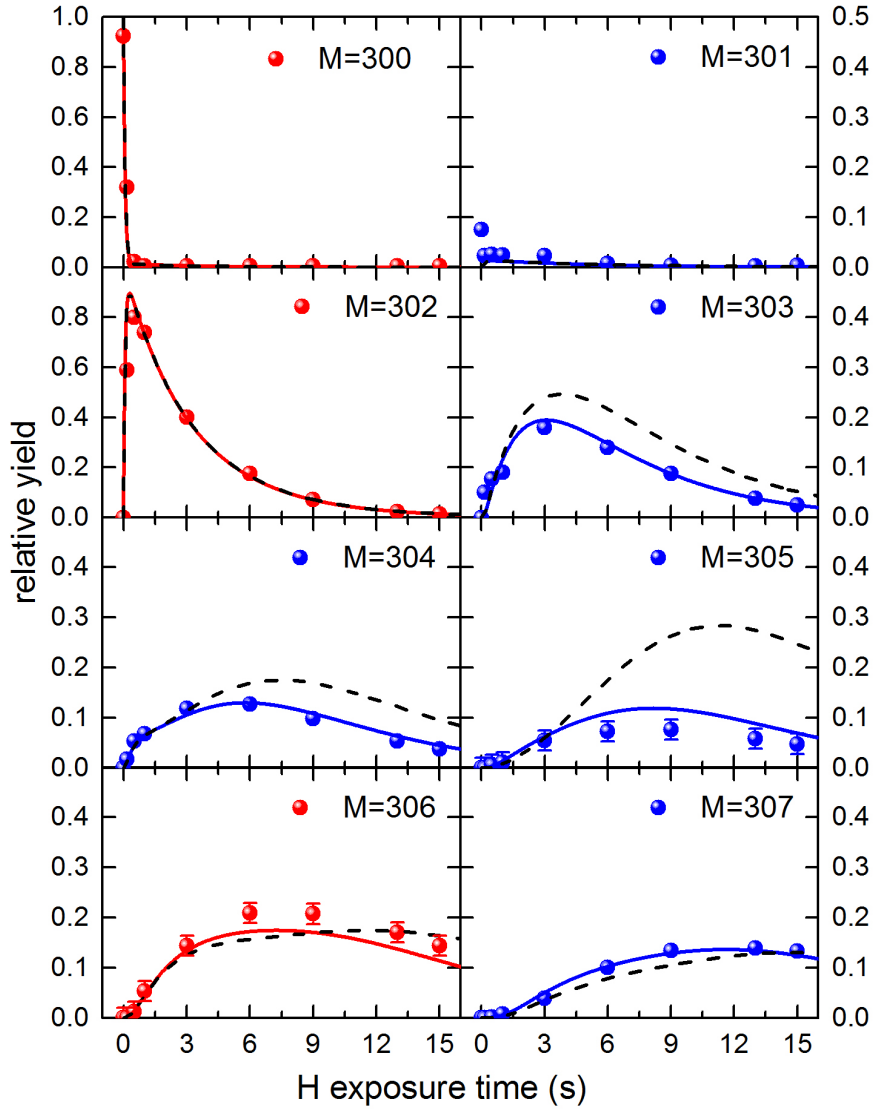
Figure 3. Ion yields for mass numbers M=300-307 Da as a function of D exposure time. Solid data points: experimental data (red: masses resulting from pure D attachment; blue: masses that necessarily involve H abstraction). Dashed lines: Simulation results obtained with abstraction cross sections for graphene. Solid: modified abstraction barriers (see text). The experimental error bars reflect uncertainties from the data treatment: background subtraction, Gaussian fitting as well as the presence of a small contamination of 13C that we could not discriminate.

abstraction cross sections had to be significantly increased to at least 0.45 Å^2 while the addition cross sections are set to 0.9 Å^2. This implies that for coronene cations, abstraction rates are at least half of addition rates. Note that since the flux of D atoms is difficult to constrain in our experiments, the cross sections derived in our model could be different. However, our model allows to derive the ratio between abstraction and addition cross sections.

Fig. 3 displays the model results for the yields of various superdeuterated coronene cations as a function of their mass number M as dashed lines. The agreement with the experimental data is good with the exception of the $M = 303$ and 305 case.

Our model gives a reliable ratio of the cross sections and thus of the reaction rates. It is important to realize that the absolute cross sections are related to the respective reaction

barriers for attachment and abstraction. Barriers and cross sections cannot be determined independently with our approach. A closer look at the dashed lines in fig. 3 reveals an overestimation of the yields for $M = 303, 304$ and 305 whereas the yields for higher masses ($M = 306, 307$) are underestimated. The two different attachment barriers $E_{attach}^{radical} = 10$ meV ($n + m$ even, radical-radical reaction) and $E_{attach}^{closed} = 30$ meV ($n + m$ odd, closed-shell-radical reaction) we used were theoretically determined for sequential hydrogenation in the absence of abstraction reactions (Cazaux et al. 2016). Abstraction reactions could induce a deviation from the hydrogenation sequence.

For instance, sequential attachment of 3 D atoms to sites 1, 2 and 3 leads to formation of $C_{24}H_{12}D_3^+$ (see fig.1, D exposure to 12 H, $n = 0$, $M = 306$). Starting from this con-

figuration, an abstraction could remove an H from one of the neighboring doubly occupied outer-edge sites, e.g. site 2 (see fig.1, the molecule shifts down-left to 11 H, $n = 1$, $M = 305$). The result is a radical configuration that would not be formed by attachment processes only, with a single doubly occupied outer edge site 1 and a singly occupied inner edge site 3. Attachment barriers typically decrease upon structural perturbations (Cazaux et al. 2016) which could result in attachment of the next D atom not only to site 2 but also to site 4. The resulting closed shell cation would have either a 1, 2, 3 conformation (with the correspondingly high attachment barrier $E_{attach}^{closed} = 30$) or it would have a 1, 3, 4 configuration. In the latter case, the attachment barrier could be lowered, because there are now two singly occupied outer edge sites with a perturbed molecular structure due to neighboring doubly occupied outer edge sites. Similar reasoning is not limited to an abstraction from the triply superhydrogenated configuration but to all configurations that have originally undergone $n \geq 2$ D attachment processes and at least one abstraction reaction.

Abstraction reactions could also reduce the barrier for subsequent attachment, because abstraction leads to extra vibrational excitation of the remaining coronene cation. For similar Eley-Rideal processes on graphite, it has been theoretically shown that most of the released energy goes into the vibrational energy of the substrate rather than into the formed H_2 (Bachellerie et al. 2007; Sizun et al. 2010). On the other hand, attachment also increases vibrational excitation and does not lead to decreasing attachment barriers.

We have tried to reflect this with our model, by lowering the attachment barriers E_{attach}^{closed} from 30 meV to 10 meV for the discussed closed shell configurations ($n \geq 2$, at least one abstraction, see appendix barriers in bold face). The resulting yields are shown in fig.3 as solid lines. The increased agreement between model results and experimental data is obvious.

While our model reproduces experimental data better when attachment barriers for all configurations modified by abstraction reactions are reduced, we would like to stress that other mechanisms cannot be ruled out. The number of potential attachment sites could be different for different configurations corresponding to the same hydrogenation state. Also, abstraction reactions could lead to an increase in internal energy.

4 CONCLUSIONS

The main conclusion from our study is therefore the 2:1 ratio between attachment and abstraction. This implies that H abstraction from gas phase coronene cations is at least more than 7 times more efficient than H abstraction from neutral coronene thin films. This could have implications for H_2 production in the ISM. For instance, Andrews *et al.* (Andrews et al. 2016) have recently shown that in photodissociation regions, PAHs only contribute to H_2 formation via photodissociation channels and not via abstraction mechanisms. However, their calculations were based on the low abstraction cross sections from (Mennella et al. 2012). An increase of the abstraction cross section by one order of magnitude could make PAHs a very important route for the formation of H_2 in space.

REFERENCES

Andrews H., Candian A., Tielens A. G. G. M., 2016, Astronomy & Astrophysics, 595, A23
Bachellerie D., Sizun M., Teillet-Billy D., Rougeau N., Sidis V., 2007, Chemical Physics Letters, 448, 223
Bari S., Gonzalez-Magana O., Reitsma G., Hoekstra R., Werner J., Schippers S., Schlathölter T., 2011, J. Chem. Phys., 134, 024314
Bauschlicher C., 1998, Astrophysical Journal, 509, L125
Bernstein M., Sandford S., Allamandola L., 1996, Astrophysical Journal, 472, L127
Boschman L., Reitsma G., Cazaux S., Schlathölter T., Hoekstra R., Spaans M., Gonzalez-Magana O., 2012, Astrophysical Journal Letters, 761, L33
Boschman L., Cazaux S., Spaans M., Hoekstra R., Schlathölter T., 2015, Astronomy & Astrophysics, 579, A72
Cazaux S., et al., 2016, Scientific Reports, 6, 19835
Egorov D., Schwob L., Lalande M., Hoekstra R., Schlathölter T., 2016, Physical Chemistry Chemical Physics, 18, 26213
Gatchell M., et al., 2015, Physical Review a, 92, 050702
Gould R., Salpeter E., 1963, Astrophysical Journal, 138, 393
Hammonds M., Pathak A., Sarre P., 2009, Phys. Chem. Chem. Phys., 11, 4458
Hirama M., Tokosumi T., Ishida T., Aihara J., 2004, Chemical Physics, 305, 307
Hoekstra R., Heer F. D., Morgenstern R., 1991, Journal of Physics B-Atomic Molecular and Optical Physics, 24, 4025
Jochims H. H., Rühl E., artel H. B., Tobita S., Leach S., 1994, Astrophysical Journal, 420, 307
Knorke H., Langer J., Oomens J., Dopfer O., 2009, Astrophysical Journal Letters, 706, L66
LePage V., Keheyan Y., Bierbaum V., Snow T., 1997, J. Am. Chem. Soc., 119, 8373
LePage V., Snow T., Bierbaum V., 2009, Astrophysical Journal, 704, 274
Ling Y., Lifshitz C., 1998, J. Phys. Chem. A, 102, 708
Mennella V., Hornekaer L., Thrower J., Accolla M., 2012, Astrophysical Journal Letters, 745, L2
Morisset S., Aguillon F., Sizun M., Sidis V., 2004, JChPh, 121, 6493
Oort J. H., van de Hulst H. C., 1946, Bull. Astron. Inst. Neth, 10, 187
Pathak A., Sarre P. J., 2008, Mon. Not. R. Astron. Soc., 391, l10
Rapacioli M., Cazaux S., Foley N., Simon A., Hoekstra R., Schlathölter T., 2018, Phys. Chem. Chem. Phys., p. (submitted)
Rauls E., Hornekaer L., 2008, Astrophysical Journal, 679, 531
Reitsma G., Boschman L., Deuzeman M. J., Gonzalez-Magana O., Hoekstra S., Cazaux S., Hoekstra R., Schlathölter T., 2014, Physical Review Letters, 113, 053002
Reitsma G., Boschman L., Deuzeman M. J., Hoekstra S., Hoekstra R., Schlathölter T., 2015, Journal of Chemical Physics, 142, 024308
Schlathölter T., Egorov D., Hoekstra R., Berden G., Oomens J., Cazaux C., 2018, to be published
Schutte W., Tielens A., Allamandola L., 1993, Astrophysical Journal, 415, 397
Sizun M., Bachellerie D., Aguillon F., Sidis V., 2010, Chemical Physics Letters, 498, 32
Skov A. L., Thrower J. D., Hornekaer L., 2014, Faraday Discuss., 168, 223
Snow T., Page V. L., Keheyan Y., V.M.Bierbaum V., 1998, Nature, 391, 259
Thrower J. D., et al., 2012, ApJ, 752, 3
Wakelam V., et al., 2017, Molecular Astrophysics, 9, 1
Wolf M., Giacomozzi L., Gatchell M., de Ruette N., Stockett

M. H., Schmidt H. T., Cederquist H., Zettergren H., 2016, European Physical Journal D, 70, 85

SUPPLEMENTARY INFORMATION

We used a simple rate equation approach to compute the deuterium addition and abstraction on/from coronene cations. The different reactions considered in our chemical network are shown in table 1. Each reaction rate is computed as R=$g \times \sigma \times \exp(\frac{-Ea}{T})$, where g is the degeneracy, Ea the reaction barrier and sigma the cross section. The formation of a species x through the reaction of y and z is described by $\frac{dn_x}{dt} = R * n_y n_z$, while the destruction of the species x through reaction with z is $\frac{dn_x}{dt} = -R * n_x n_z$. The addition and abstraction cross sections reproducing the experimental measurements are listed in the table.

Table 1. Cross sections, barriers and degeneracies for the various attachment and abstraction channels as used for the numerical modeling leading to the solid lines in fig.3.

initial PAH	incoming atom	final PAH	abstraction product	cross section (Å^2)	reaction barrier	degeneracy	initial mass	final mass
Cor^+	D	$CorD^+$		0.9	0.010	12	300	302
$CorD^+$	D	Cor^+	D2	0.45	0.010	1	302	300
$CorD^+$	D	$CorD_2^+$		0.9	0.030	1	302	304
$CorD^+$	D	$(CorD\text{-}H)^+$	HD	0.45	0.010	1	302	301
$(CorD\text{-}H)^+$	D	$(CorD_2\text{-}H)^+$		0.9	0.010	12	301	303
$CorD_2^+$	D	$CorD^+$	D_2	0.45	0.010	2	304	302
$CorD_2^+$	D	$CorD_3^+$		0.9	0.010	4	304	306
$CorD_2^+$	D	$(CorD_2\text{-}H)^+$	HD	0.45	0.010	2	304	303
$(CorD_2\text{-}H)^+$	D	$(CorD\text{-}H)^+$	D_2	0.45	0.010	1	303	301
$(CorD_2\text{-}H)^+$	D	$(CorD_3\text{-}H)^+$		0.9	**0.030/0.010**	1	303	305
$(CorD_2\text{-}H)^+$	D	$(CorD_2\text{-}H_2)^+$	HD	0.45	0.010	1	303	302
$(CorD_2\text{-}H_2)^+$	D	$(CorD_3\text{-}H_2)^+$		0.9	0.010	12	302	304
$CorD_3^+$	D	$CorD_2^+$	D_2	0.45	0.010	1	306	304
$CorD_3^+$	D	$CorD_4^+$		0.9	0.030	1	306	308
$CorD_3^+$	D	$(CorD_3\text{-}H)^+$	HD	0.45	0.010	1	306	305
$(CorD_3\text{-}H)^+$	D	$(CorD2\text{-}H)^+$	D_2	0.45	0.010	2	305	303
$(CorD_3\text{-}H)^+$	D	$(CorD_4\text{-}H)^+$		0.9	0.010	4	305	307
$(CorD_3\text{-}H)^+$	D	$(CorD_3\text{-}H_2)^+$	HD	0.45	0.010	2	305	304
$(CorD_3\text{-}H_2)^+$	D	$(CorD2\text{-}H_2)^+$	D_2	0.45	0.010	1	304	302
$(CorD_3\text{-}H_2)^+$	D	$(CorD_4\text{-}H_2)^+$		0.9	**0.030/0.010**	1	304	306
$(CorD_3\text{-}H_2)^+$	D	$(CorD_3\text{-}H_3)^+$	HD	0.45	0.010	1	304	303
$(CorD_3\text{-}H_3)^+$	D	$(CorD_4\text{-}H_3)^+$		0.9	0.010	12	303	305
$CorD_4^+$	D	$CorD3^+$	D_2	0.45	0.010	4	308	306
$CorD_4^+$	D	$CorD5^+$		0.9	0.010	1	308	310
$CorD_4^+$	D	$(CorD_4\text{-}H)^+$	HD	0.45	0.010	4	308	307
$(CorD_4\text{-}H)^+$	D	$(CorD_3\text{-}H)^+$	D_2	0.45	0.010	3	307	305
$(CorD_4\text{-}H)^+$	D	$(CorD_5\text{-}H)^+$		0.9	**0.030/0.010**	1	307	309
$(CorD_4\text{-}H)^+$	D	$(CorD_4\text{-}H_2)^+$	HD	0.45	0.010	3	307	306
$(CorD_4\text{-}H_2)^+$	D	$(CorD_3\text{-}H_2)^+$	D_2	0.45	0.010	2	306	304
$(CorD_4\text{-}H_2)^+$	D	$(CorD5\text{-}H_2)^+$		0.9	0.010	4	306	308
$(CorD_4\text{-}H_2)^+$	D	$(CorD_4\text{-}H_3)^+$	HD	0.45	0.010	2	306	305
$(CorD_4\text{-}H_3)^+$	D	$(CorD_3\text{-}H_3)^+$	D_2	0.45	0.010	1	305	303
$(CorD_4\text{-}H_3)^+$	D	$(CorD_5\text{-}H_3)^+$		0.9	**0.030/0.010**	1	305	307
$(CorD_4\text{-}H_3)^+$	D	$(CorD_4\text{-}H_4)^+$	HD	0.45	0.010	1	305	304
$(CorD_4\text{-}H_4)^+$	D	$(CorD_5\text{-}H_4)^+$		0.9	0.010	12	304	306
$CorD_5^+$	D	$CorD_4^+$	D_2	0.45	0.010	5	310	308
$CorD_5^+$	D	$CorD_6^+$		0.9	0.100	4	310	312
$CorD_5^+$	D	$(CorD_5\text{-}H)^+$	HD	0.45	0.010	5	310	309
$(CorD_5\text{-}H)^+$	D	$(CorD_4\text{-}H)^+$	D_2	0.45	0.010	4	309	307
$(CorD_5\text{-}H)^+$	D	$(CorD_6\text{-}H)^+$		0.9	0.010	1	309	311
$(CorD_5\text{-}H)^+$	D	$(CorD5\text{-}H_2)^+$	HD	0.45	0.010	4	309	308
$(CorD_5\text{-}H_2)^+$	D	$(CorD_4\text{-}H_2)^+$	D_2	0.45	0.010	3	308	306
$(CorD_5\text{-}H_2)^+$	D	$(CorD_6\text{-}H2)^+$		0.9	0.030	1	308	310
$(CorD_5\text{-}H_2)^+$	D	$(CorD_5\text{-}H_3)^+$	HD	0.45	0.010	3	308	307
$(CorD_5\text{-}H_3)^+$	D	$(CorD_4\text{-}H_3)^+$	D_2	0.45	0.010	2	307	305
$(CorD_5\text{-}H_3)^+$	D	$(CorD_6\text{-}H_3)^+$		0.9	0.010	4	307	309
$(CorD_5\text{-}H_3)^+$	D	$(CorD_5\text{-}H_4)^+$	HD	0.45	0.010	2	307	306
$(CorD_5\text{-}H_4)^+$	D	$(CorD_4\text{-}H_4)^+$	D_2	0.45	0.010	1	306	304
$(CorD_5\text{-}H_4)^+$	D	$(CorD_6\text{-}H_4)^+$		0.9	0.030	1	306	308
$(CorD_5\text{-}H_4)^+$	D	$(CorD_5\text{-}H_5)^+$	HD	0.45	0.010	1	306	305
$(CorD_5\text{-}H_5)^+$	D	$(CorD_6\text{-}H_5p$		0.9	0.010	12	305	307
$CorD_6^+$	D	$CorD_5^+$	D_2	0.45	0.010	6	312	310
$CorD_6^+$	D	$CorD_7^+$		0.9	0.010	1	312	314
$CorD_6^+$	D	$(CorD_6\text{-}H)^+$	HD	0.45	0.010	6	312	311
$(CorD_6\text{-}H)^+$	D	$(CorD_5\text{-}H)^+$	D_2	0.45	0.010	5	311	309
$(CorD_6\text{-}H)^+$	D	$(CorD_7\text{-}H)^+$		0.9	0.100	1	311	313
$(CorD_6\text{-}H)^+$	D	$(CorD_6\text{-}H_2)^+$	HD	0.45	0.010	5	311	310
$(CorD_6\text{-}H_2)^+$	D	$(CorD_5\text{-}H_2)^+$	D_2	0.45	0.010	4	310	308
$(CorD_6\text{-}H_2)^+$	D	$(CorD_7\text{-}H_2)^+$		0.9	0.010	1	310	312
$(CorD_6\text{-}H_2)^+$	D	$(CorD_6\text{-}H_3)^+$	HD	0.45	0.010	4	310	309
$(CorD_6\text{-}H_3)^+$	D	$(CorD_5\text{-}H_3)^+$	D_2	0.45	0.010	3	309	307
$(CorD_6\text{-}H_3)^+$	D	$(CorD_7\text{-}H_3)^+$		0.9	0.030	1	309	311
$(CorD_6\text{-}H_3)^+$	D	$(CorD_6\text{-}H4)^+$	HD	0.45	0.010	3	309	308
$(CorD_6\text{-}H_4)^+$	D	$(CorD_5\text{-}H4)^+$	D_2	0.45	0.010	4	308	306
$(CorD_6\text{-}H_4)^+$	D	$(CorD_7\text{-}H4)^+$		0.9	0.010	2	308	310
$(CorD_6\text{-}H_4)^+$	D	$(CorD_6\text{-}H_5)^+$	HD	0.45	0.010	4	308	307
$(CorD_6\text{-}H_5)^+$	D	$(CorD5\text{-}H_5)^+$	D_2	0.45	0.010	1	307	305
$(CorD_6\text{-}H_5)^+$	D	$(CorD_7\text{-}H_5)^+$		0.9	0.030	1	307	309
$(CorD_6\text{-}H_5)^+$	D	$(CorD_6\text{-}H_6)^+$	HD	0.45	0.010	1	307	306
$(CorD_6\text{-}H_6)^+$	D	$(CorD_7\text{-}H_6)^+$		0.9	0.010	12	306	308